ORIGINAL ARTICLE

Synthesis of nitrogen mustard-based fluorophores for cell imaging and cytotoxicity studies

Yuanwei Liang, Maojun Liang, Cuiyu Li, Daini Wang, Xiaoxuan Gong, Kaiji Zheng

Department of Chemistry, Guangdong Ocean University, Zhanjiang, China

J. Adv. Pharm. Technol. Res.

ABSTRACT

Nitrogen mustards are important alkylating anticancer drugs used for neoplasms treatment. However, little research about the integration of luminophore into nitrogen mustard-based compounds for both imaging and therapeutic application was reported. In this study, we report a series of novel nitrogen mustard-containing 1-furyl-2-en-1-one and 1-thienyl-2-en-1-one derivatives as intramolecular charge transfer-based luminophore for research in both imaging subcellular localization and antiproliferation toward lung cancer cells. The target products were prepared by Knoevenagel condensation and characterized by nuclear magnetic resonance and high-resolution mass spectrometer. The absorption and fluorescence studies were carried out by ultraviolet-visible and fluorescence spectrophotometers, respectively. Cell morphology was observed under an inverted microscope. Cytotoxicity test was detected by MTT assay. Cellular localization was observed by a confocal laser scanning microscope. Colony formation ability was carried out by colony formation assay. Cell migration ability was detected by transwell migration assay. Differences between the two groups were analyzed by two-tailed Student's *t*-test. The difference with $P < 0.05$ (*) was considered statistically significant. The compounds were synthesized in high yield. The λ_{max} and Stokes shift of these compounds reach up to 567 and 150 nm, respectively. These compounds exhibited good antiproliferative activity against lung cancer cells, with compound 3h exhibiting the best IC_{50} of 13.1 ± 2.7 μM. Furthermore, the selected compound 3h is located preferentially in lysosomes and a small amount in nuclei, effectively inhibiting cell colony formation and migration abilities toward A549 cells. These findings suggested that nitrogen mustard-based fluorophores might be a potential effective chemotherapeutic agent in lung cancer therapy.

Key words: Cell migration, cytotoxicity, fluorophore, nitrogen mustard

INTRODUCTION

Cancer is one of the leading causes of death worldwide,[1] among which lung cancer has become one of the most common forms.[2] Therefore, anticancer agent exploitation derived from artificial synthesis and their derivatives for lung cancer prevention and therapeutics are imperative.

Address for correspondence:
Dr. Yuanwei Liang,
Department of Chemistry, Guangdong Ocean University, No. 1, Haida Road, Mazhang District, Zhanjiang City, China.
E-mail: liangyw@gdou.edu.cn

Submitted: 11-Sep-2022 **Revised:** 27-Sep-2022
Accepted: 19-Oct-2022 **Published:** 20-Jan-2023

Access this article online	
Quick Response Code:	Website: www.japtr.org
	DOI: 10.4103/japtr.japtr_574_22

How to cite this article: Liang Y, Liang M, Li C, Wang D, Gong X, Zheng K. Synthesis of nitrogen mustard-based fluorophores for cell imaging and cytotoxicity studies. J Adv Pharm Technol Res 2023;14:6-11.

In recent years, the development of fluorescent probes has become a research hotspot that springs up exuberantly, and they are often used for the purpose of enabling the research of biological processes in cancer treatment, such as real-time biomolecular imaging and diagnostics.[3-5] Meanwhile, research in anticancer drugs with therapeutic moiety and luminophore moiety has been well developed.[6,7] Such drugs play a dual role: diagnosis and treatment. They can be used not only for real-time imaging but also as a therapeutic agent.[8] However, many treatment agents turn to lack effective luminescent units generating valid fluorescence. Although there are many fluorescent molecules emerging continuously, the stokes shift turn to be small and the emission wavelength is generally short.[9,10] Among various probes, intramolecular charge transfer (ICT)-based organic molecules are widely used for several technological applications,[11] such organic light-emitting diodes,[12] dye-sensitized solar cells[13] and biomedicine materials.[14] ICT probe is consisted of a strong electron-withdrawing group and a strongly pushed electron base, and mostly with a p-electron bridge between them, forming a D-π-A system.[15] Many of them are featured with relatively long emission wavelengths and large stokes shift.

Nitrogen mustards are important alkylating anticancer drugs, which have been used for a variety of solid neoplasms treatment,[16] especially in lung and breast cancers.[17,18] Over the past decades, a good deal of modifications have been made in the area of nitrogen mustard agent to improve its therapeutic effect due to its high reactivity and peripheral cytotoxicity. However, little research about the integration of luminophore into the nitrogen mustard-containing structure for imaging as auxiliary functions of therapeutic effect was reported.

In this study, we report a series of novel nitrogen mustard-containing 1-furyl-2-en-1-one and 1-thienyl-2-en-1-one derivatives as ICT-based luminophores for research in both imaging subcellular localization and antiproliferation toward lung cancer cells. Here, nitrogen mustard was served as a strongly pushed electron base and the carbonyl as electron-withdrawing group. Their optical properties, including ultraviolet (UV)-visible and fluorescence spectrum, were studied. Their antiproliferative activity against lung cancer cells, effects on cell colony formation and migration as well as intracellular localization were investigated.

MATERIALS AND METHODS

General synthetic pathway of the compounds (3a~3k)

As Scheme 1 shown, DMF (40 mmol) was mixed with $POCl_3$ (20 mmol) upon stirring at 0°C–4°C for 20 min under N_2 atmosphere. 1 (5 mmol) in DMF (2 mL) upon stirring was added above mixture slowly, then heat at 100°C for 3 h, cool to 25° and poured it into ice water (150 mL), neutralized with NaOH solution, then filtered and

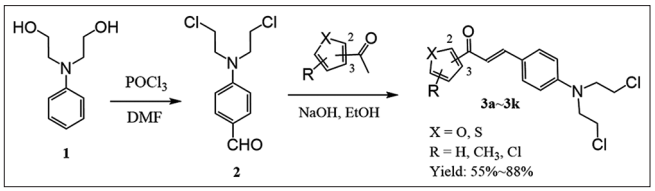

Scheme 1: Synthetic pathway of compounds 3a–3k

washed with MeOH/H_2O (1:1, v/v), recrystallized from MeOH/CH_2Cl_2 (1:1, v/v) to give 2. To a solution of 2 (0.3 mmol) and different substituted acetylthiophene or acetylfuran in EtOH (5 mL) upon stirring was added NaOH (0.4 mmol) to react at 25° for 24 h. Removed the solvent, the residue was subjected to column chromatography (CH_2Cl_2/CH_3OH = 50:1, v/v) to give the 3a–3k.[19]

Absorption and fluorescence studies

3a–3k were dissolved in ethanol, the UV–visible spectra and emission spectra were obtained by a Puxi TU-1901 UV-visible spectrophotometer and a Hitachi F-2500 fluorescence spectrophotometer, respectively.

Assessment of cell viability

Adherent cells were incubated with different concentrations of compounds at 37°C for 72 h. Then 25 μL of MTT reagent was added and incubated for 3h. The medium was removed and 150 uL of DMSO was added to dissolve the formazan. Read the plate at OD_{570} by a microplate reader.[20]

Cellular morphology

Cells were seeded in 2 cm dishes (2×10^5 cells/dish) and incubated with 3h (10 μM or 20 μM) for 48 h, then removed the culture medium washed cells with PBS, and cell morphology was observed under an inverted microscope.

Subcellar location

Cells were incubated with 3 h (20 μM, for 3 h), Lyso-Tracker Red (1 μM, for 1 h), and Hoechst 33342 (1 μM, for 0.5 h) at 37°C. The medium was removed and washed with PBS, and another PBS (2 mL) was added. Fluorescent signals in cells were examined using a confocal laser scanning microscope (Olympus FluoView FV1000).[21]

Colony formation assay

Cells were seeded into 6-well cell culture plates (400 cells/well), then incubated with 3 h for 12 days, until visible colonies can be witnessed in the control group, washed cells mildly with PBS for twice, fixed cells with 4% paraformaldehyde solution, then stained cells with 0.2% crystal violet for 15 min and counted the stained colonies.[22]

Transwell migration assay

After cells were incubated with 3 h for 48 h, removed the medium and washed with PBS, resuspended cells with serum-free medium, and seeded them (5×10^4 cells) into the upper chamber supplement, coated the upper chambers

with Matrigel, added the medium (1 mL) to the lower chamber and cultured in a 24-well plate for 24 h. Extracted the transwell chamber, fixed with methanol, and stained cells with 0.1% of crystal violet. Cells were photographed and counted by a microscope.[23]

RESULTS

The novel compounds 3a–3k were synthesized in high yield (55%~88%). Their λ_{em} and Stokes shift was up to 567 nm and 150 nm, respectively. These compounds exhibited good antiproliferative activity against lung cancer cells, with IC_{50} of 13.1 ± 2.7 to 33.5 ± 2.6 μM against A549 cells and 14.2 ± 3.3 to 29.8 ± 0.9 μM against NCI-H460 cells. Selected compound 3h is located preferentially in lysosomes and a small amount in nuclei. Furthermore, 3h effectively inhibited cell colony formation and migration abilities toward A549 cells.

DISCUSSION

Their structures of the synthetic compounds is displayed in Figure 1, which were characterized by NMR and High-Resolution Mass Spectrometer as supplemented in Supporting Information.

The absorption and fluorescence spectra are shown in Figure 2, the λ_{max}, $\lambda_{em,}$ and Stokes shift is recorded in Table S1. Compounds 3c and 3k showed relatively short λ_{max} (392 nm and 399 nm, respectively), demonstrating that carbonyl group substituted in 2-position possessed longer λ_{max} than in the 3-position. In addition, Cl-substituted products (3h, 3i, and 3j) present longer λ_{max} than CH_3-substituted ones. Similarly, 3c and 3k possess corresponding shorter λ_{em} than other compounds, whereas Cl-substituted products showed longer λ_{em} among all compounds, with λ_{em} up to 566 nm, 563 nm, and 567 nm, respectively. The Stokes shift of all compounds is also large, although a great difference exists. Compound 3b demonstrates correspondingly short Stokes shift, only 113 nm. The largest Stokes shift belongs to compound 3j, up to 150 nm. These results demonstrate the excellent fluorescence property of the synthetic compounds.

The cytotoxicity of 3a–3k against two lung cancer cell lines (NCI-H460 and A549) is shown in Figure 3; their 50% inhibiting concentration (IC_{50}, μM) was calculated and presented in Table S2. Specifically, most compounds displayed good activity against the two tested cervical cancer cell lines after 72 h treatment. In terms of NCI-460 cells, 3a–3g exhibits correspondingly low cytotoxic activity, with IC_{50} from 23.1 ± 1.4 to 29.8 ± 0.9 μM. The introduction of an electron-donor group, such as methyl in furan or thiophene, did not conspicuously change the cytotoxic activity. Whereas a significant increase in cytotoxic activity was witnessed, no matter where the chlorine was substituted in 3-, 4-, or 5-position, since 3h, 3i, and 3j were found to be more potent than other compounds, with IC_{50} only 16.6 ± 0.9, 14.2 ± 3.3, and 15.0 ± 2.2 μM, respectively. Similarly, 3a–3g, without or with methyl-substituted in different positions, exerts relatively weak activity against A549 cells, with IC_{50} of 26.3 ± 2.8 to 33.5 ± 2.6 μM. Nevertheless, the introduction of chlorine atom significantly enhanced the activity by even more than double compared to 3d, a product with no substitution in thiophene, with IC_{50} of 13.1 ± 2.7, 17.1 ± 4.8 and 14.6 ± 3.2 μM, respectively. The results indicate the good anticancer activity of the synthetic compounds. As 3h exhibited the best activity on A549 cells, its anticancer activity was investigated further.

Cell morphology was observed under optical microscope after incubation with selected compound 3h, as it is shown in Figure 4 that treating A549 cells with 3h give rise to oncotic necrosis. Furthermore, lower adhesion and protuberance retract or disappear can be witnessed. This result demonstrates a programmed cell death.

The subcellular localization of ICT-based luminophore 3h in cells was detected by confocal laser scanning microscope, as shown in Figure 5. A549 cells were co-stained with Lyso-Tracker Red probe, cell nucleus probe Hoechst 33342 in company with 3h together. The blue of Hoechst 33342, the bright green of 3h and the red of Lyso-Tracker can be seen in Figure 5. As they merge, a well overlap between 3h and Lyso-Tracker can be witnessed. Meanwhile, a small amount of green fluorescence signal was found to overlap with blue

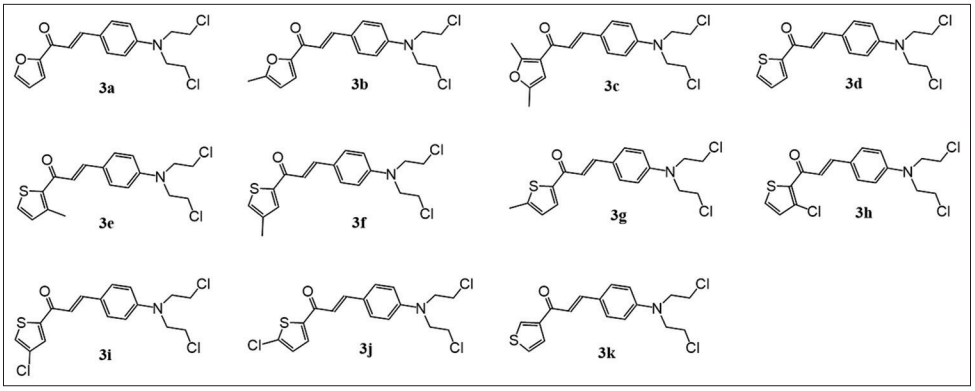

Figure 1: Chemical structure of 3a–3k

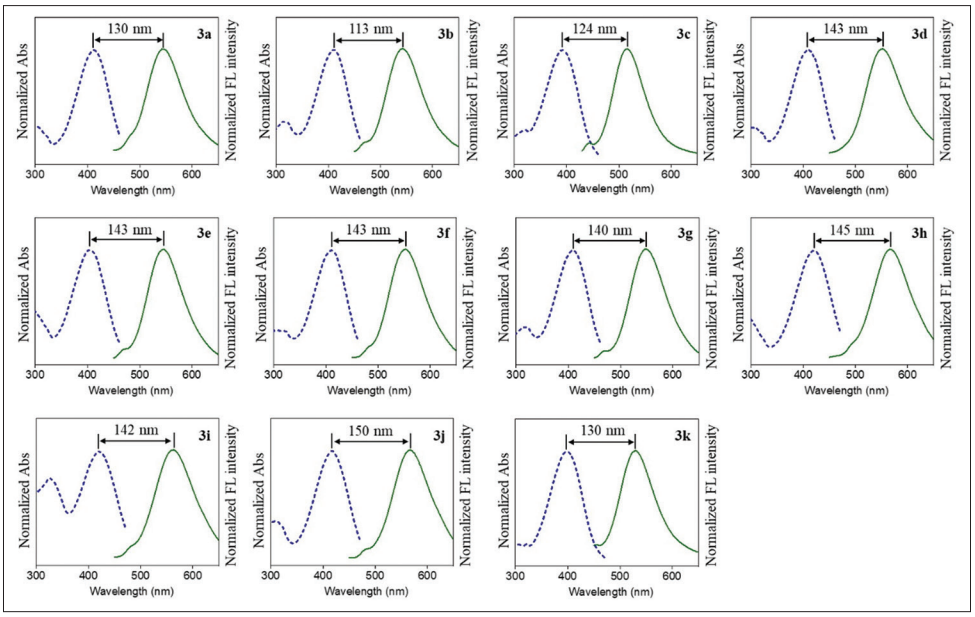

Figure 2: Absorption (dotted line), fluorescence spectra (solid line) and Stokes shift of 3a–3k. Compounds was dissolved in EtOH and λmax was set as excitation wavelength per fluorescence spectrum

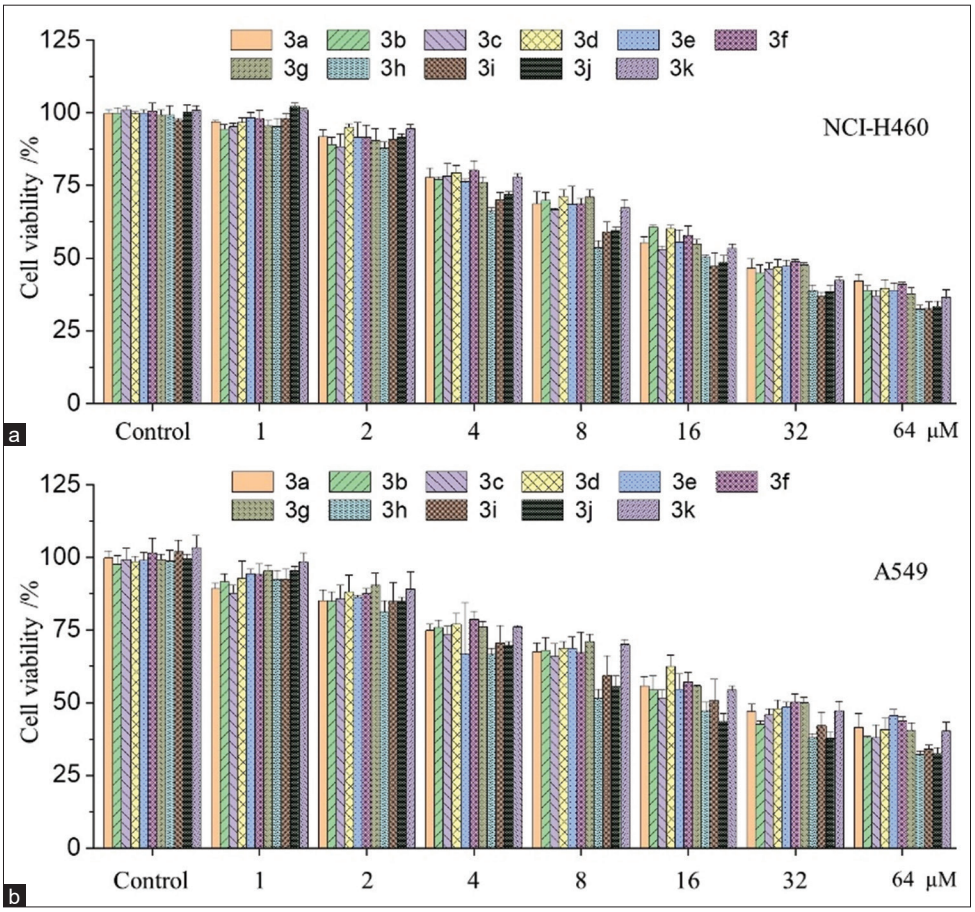

Figure 3: Anti-proliferative activity of 3a–3k against NCI-H460 (a) and A549 (b) lung cancer cell lines. Cells were treated with increasing concentration of 3a–3k. Cell viability was measured using MTT assay

signal. This indicates that 3h is located preferentially in lysosomes and a small amount in nuclei.

The inhibitory effect of 3h on the colony formation ability of A549 cells was detected by colony formation assay, as

shown in Figure 6a and statistically analyzed in Figure 6b. The colony number of A549 cells was reduced to 127 ± 5.6 when treated with 10 μM of 3h, which was obviously smaller than 161 ± 2.9, the colony number of the control group. This tendency became more significant when it does rise to 20 μM and the colony number declined to only 75 ± 2.8, even less than half of the control group. This result suggests that 3h significantly reduced the colony formation ability of A549 cells.

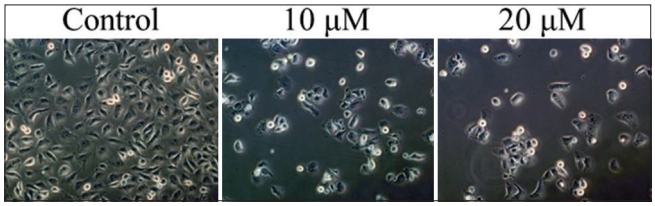

Figure 4: Cellular morphology of A549 cell. Cell was incubated with 3h (10 or 20 μM) for 48 h, then cell morphology was observed under an inverted microscope

The inhibitory effects of 3h on the migration ability of A549 cells are displayed in Figure 7a and statistically analyzed in Figure 7b. Results showed that 3h treated cells significantly suppressed the migration of A549 cells. Comparing to the control group of cell number (195 ± 7.7), the treatment group (10 μM) witnesses an obvious decline, only 99 ± 4.3 cells, which is only nearly half of the control group. When cells were treated with of 20 μM of 3h, the cell number was further reduced to 70 ± 3.7. These data suggest that 3h treatment suppresses the migratory abilities of A549 cells.

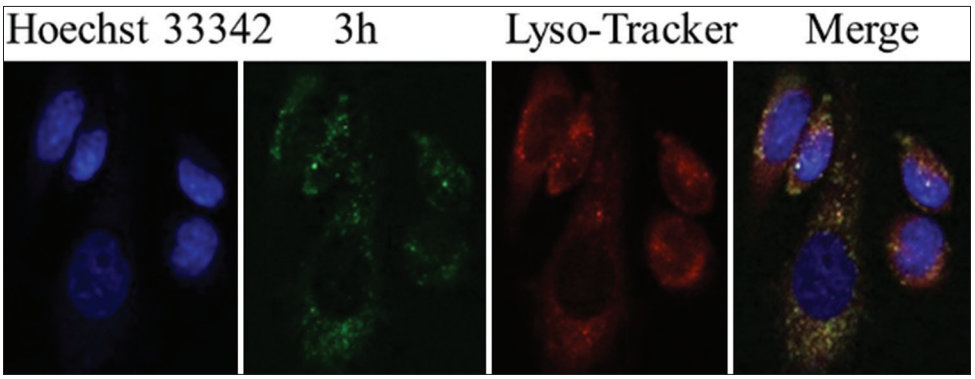

Figure 5: CLSM observation of cellular localization of 3h in A549 cells for subcellular localization investigation. Cells were incubated with 3h (for 4 h) then stained with Lyso-Tracker red (for 1 h) and Hoechst 33342 (for 0.5 h) then imaging was performed by CLSM. CLSM: Confocal laser scanning microscope

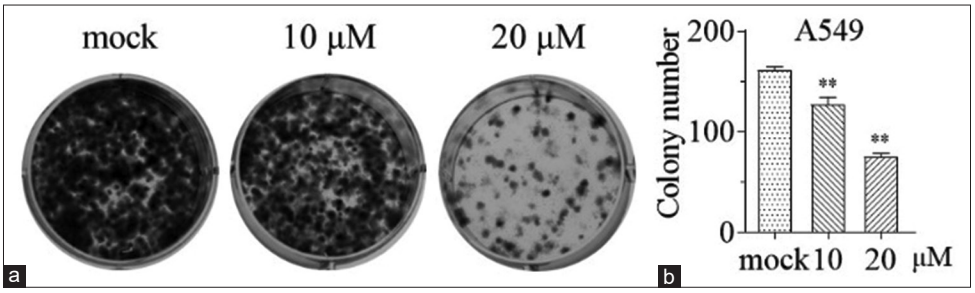

Figure 6: Cell colony formation assay results. (a) Represented images of colony formation assay in A549, after exposure with 10 and 20 μM of 3h. (b) Statistical analysis of counted colony number in A549 cells. $^{**}P < 0.01$

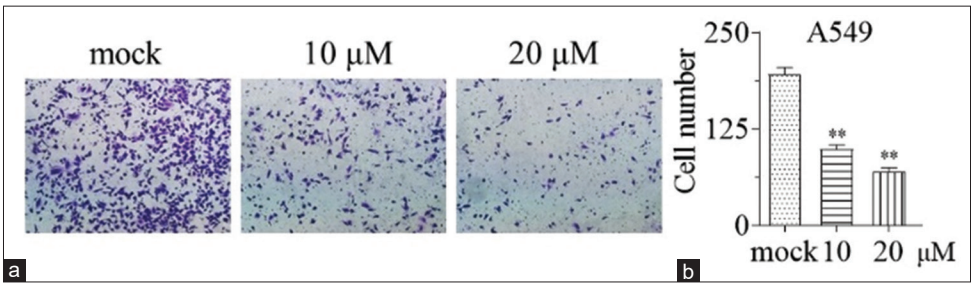

Figure 7: Inhibitory effects of 3h on migration ability of A549 cells. (a) A549 cells were treated with 10 and 20 μM of 3h and then subjected to cell migration assay. (b) Statistical analysis of migration cell number. $^{**}P < 0.01$

CONCLUSSIONS

A series of novel ICT-based fluorophore that contains nitrogen mustard for both cellular imaging and the anticancer investigation was developed. The 11 compounds exhibited long λ_{em} and Stokes shift. These compounds exhibited good anticancer activity against lung cancer cells NCI-H460 and A549, among which the chlorine atom substituted in the thiophene ring products turned out to be the best active. As one of the best active compounds, 3h effectively inhibited cell proliferation, colony formation abilities, and migration against A549 cells. In addition, 3h was located preferentially in lysosomes and a small amount in nuclei. This study provides a resultful reference for promising development in nitrogen mustard conjugates with anticancer activity and fluorescence imaging.

Financial support and sponsorship

This work was funded by the GuangDong Basic and Applied Basic Research Foundation (2019A1515110313), the Science and Technology Plan Project of Zhanjiang City (2019A01012, 2021A05045), Program for Scientific Research Start-up Funds of Guangdong Ocean University (R19057).

Conflicts of interest

There are no conflicts of interest.

REFERENCES

1. Miller KD, Nogueira L, Devasia T, Mariotto AB, Yabroff KR, Jemal A, *et al.* Cancer treatment and survivorship statistics, 2022. CA Cancer J Clin 2022;72:409-36.
2. Siegel RL, Miller KD, Fuchs HE, Jemal A. Cancer statistics, 2022. CA Cancer J Clin 2022;72:7-33.
3. Wu Y, Balasubramanian P, Wang Z, Coelho JA, Prslja M, Siebert R, *et al*. Detection of few hydrogen peroxide molecules using self-reporting fluorescent nanodiamond quantum sensors. J Am Chem Soc 2022;144:12642-51.
4. Ma H, Lu Y, Huang Z, Long S, Cao J, Zhang Z, *et al.* ER-targeting cyanine dye as an NIR photoinducer to efficiently trigger photoimmunogenic cancer cell death. J Am Chem Soc 2022;144:3477-86.
5. Chen HJ, Qin Y, Wang ZG, Wang L, Pang DW, Zhao D, *et al.* An activatable and reversible virus-mimicking NIR-II nanoprobe for monitoring the progression of viral encephalitis. Angew Chem Int Ed Engl 2022;61:e202210285.
6. Han J, Li H, Zhao L, Kim G, Chen Y, Yan X, *et al.* Albumin-mediated "Unlocking" of supramolecular prodrug-like nanozymes toward selective imaging-guided phototherapy. Chem Sci 2022;13:7814-20.
7. Wang Y, Shi X, Fang H, Han Z, Yuan H, Zhu Z, *et al.* Platinum-based two-photon photosensitizer responsive to NIR light in tumor hypoxia microenvironment. J Med Chem 2022;65:7786-98.
8. Gao Z, Jia S, Ou H, Hong Y, Shan K, Kong X, *et al.* An activatable near-infrared afterglow theranostic prodrug with self-sustainable magnification effect of immunogenic cell death. Angew Chem Int Ed Engl 2022;61:e202209793.
9. Fu Y, Finney NS. Small-molecule fluorescent probes and their design. RSC Adv 2018;8:29051-61.
10. Jun JV, Chenoweth DM, Petersson EJ. Rational design of small molecule fluorescent probes for biological applications. Org Biomol Chem 2020;18:5747-63.
11. Wang C, Chi W, Qiao Q, Tan D, Xu Z, Liu X. Twisted intramolecular charge transfer (TICT) and twists beyond TICT: From mechanisms to rational designs of bright and sensitive fluorophores. Chem Soc Rev 2021;50:12656-78.
12. Goes M, Verhoeven JW, Hofstraat H, Brunner K. OLED and PLED devices employing electrogenerated, intramolecular charge-transfer Fluorescence. Chemphyschem 2003;4:349-58.
13. Chordiya K, Ali ME, Kahaly MU. Photoexcited intramolecular charge transfer in dye sensitizers: Predictive *in silico* screening for dye-sensitized solar cell devices. ACS Omega 2022;7:13465-74.
14. Vayá I, Andreu I, Lence E, González-Bello C, Consuelo Cuquerella M, Navarrete-Miguel M, *et al.* Characterization of locally excited and charge-transfer states of the anticancer drug lapatinib by ultrafast spectroscopy and computational studies. Chemistry 2020;26:15922-30.
15. Li T, Guo H, Wang Y, Ouyang G, Wang QQ, Liu M. Chiral macrocycle-induced circularly polarized luminescence of a twisted intramolecular charge transfer dye. Chem Commun (Camb) 2021;57:13554-7.
16. Brulikova L, Hlavac J, Hradil P. DNA interstrand cross-linking agents and their chemotherapeutic potential. Curr Med Chem 2012;19:364-85.
17. Highley MS, Landuyt B, Prenen H, Harper PG, De Bruijn EA. The nitrogen mustards. Pharmacol Rev 2022;74:552-99.
18. Maliszewski D, Wróbel A, Kolesińska B, Frączyk J, Drozdowska D. 1,3,5-triazine nitrogen mustards with different peptide group as innovative candidates for AChE and BACE1 inhibitors. Molecules 2021;26:3942.
19. Chen H, Zhang Z, Hu T, Zhang X. Nanochannel {InZn}-organic framework with a high catalytic performance on CO_2 chemical fixation and deacetalization-knoevenagel condensation. Inorg Chem 2021;60:16429-38.
20. Ambarwati NS, Armandari MO, Widayat W, Desmiaty Y, Elya B, Arifianti AE, *et al. In vitro* studies on the cytotoxicity, elastase, and tyrosinase inhibitory activities of tomato (*Solanum lycopersicum* Mill.) extract. J Adv Pharm Technol Res 2022;13:182-6.
21. Liang Y, Huang W, Situ Q, Su W, Qiu W, Li S, *et al.* Novel Terpyridine conjugated nitrogen mustard derivatives: Synthesis, spectral properties, and anticancer activity. Russ J Gen Chem 2022;92:725-31.
22. Xin YB, Li JJ, Zhang HJ, Ma J, Liu X, Gong GH, *et al.* Synthesis and characterisation of (Z)-styrylbenzene derivatives as potential selective anticancer agents. J Enzyme Inhib Med Chem 2018;33:1554-64.
23. Ma LY, Zheng YC, Wang SQ, Wang B, Wang ZR, Pang LP, *et al.* Design, synthesis, and structure-activity relationship of novel LSD1 inhibitors based on pyrimidine-thiourea hybrids as potent, orally active antitumor agents. J Med Chem 2015;58:1705-16.

SUPPLEMENTARY FILE

Supporting information: Characterization data of the synthetic compounds

3a: Yellow solid, yield 75%. ^{1}H NMR (600 MHz, DMSO-d_6) δ: 8.02 (d, J = 1.90 Hz, 1H, Furan-H), 7.71–7.65 (overlapped, 4H, CH, Furan-H, ArH), 7.45 (d, J = 15.61 Hz, 1H, CH), 6.83(d, J = 8.89 Hz, 2H, ArH), 6.76 (dd, J = 1.90, 3.55 Hz, 1H, Furan-H), 3.84–3.76 (overlapped, 8H, CH_2). ^{13}C NMR (150 MHz, DMSO-d_6) δ: 177.19, 153.77, 149.19, 148.15, 143.86, 131.38, 123.36, 118.70, 117.35, 113.04, 112.40, 52.24, 41.53. HR-MS (ESI) m/z: Calcd for $C_{17}H_{18}Cl_2NO_2$ $[M + H]^+$ 338.0715, found 338.0716

3b: Yellow solid, yield 76%. ^{1}H NMR (600 MHz, DMSO-d_6) δ: 7.68 (d, J = 8.90 Hz, 2H, ArH), 7.64–7.60(overlapped, 2H, Furan-H, CH), 7.40(d, J = 15.52 Hz, 1H, CH), 6.83(d, J = 8.90 Hz, 2H, ArH), 6.40(dd, J = 0.90 Hz, 3.44 Hz, 1H, Furan-H), 3.84–3.76(overlapped, 8H, CH_2). ^{13}C NMR (150 MHz, DMSO-d_6) δ: 176.43, 158.21, 152.68, 149.03, 143.16, 131.23, 123.47, 120.54, 117.49, 112.37, 109.73, 52.24, 41.54, 14.19. HR-MS (ESI) m/z: Calcd for $C_{18}H_{20}Cl_2NO_2$ $[M + H]^+$ 352.0871, found 352.0873.

3c: Yellow solid, yield 70%. ^{1}H NMR (600 MHz, DMSO-d_6) δ: 7.67 (d, J = 8.90 Hz, 2H, ArH), 7.54 (d, J = 15.53 Hz, 1H, CH), 7.24 (d, J = 15.53 Hz, 1H, CH), 6.81 (d, J = 8.90 Hz, 2H, ArH), 6.73(s, J = 3.44 Hz, 1H, Furan-H), 3.82–3.77 (overlapped, 8H, CH_2). ^{13}C NMR (150 MHz, DMSO-d_6) δ: 185.25, 156.86, 150.01, 149.01, 143.22, 131.27, 123.60, 123.02, 120.15, 112.42, 106.76, 52.30, 41.59, 14.54, 43.51. HR-MS (ESI) m/z: Calcd for $C_{19}H_{22}Cl_2NO_2$ $[M + H]^+$ 366.1028, found 366.1026

3d: Yellow solid, yield 88%. ^{1}H NMR (600 MHz, DMSO-d_6) δ: 8.25 (d, J = 3.78 Hz, 1H, thiophene-H), 8.00 (d, J = 4.88 Hz, 1H, CH), 7.74 (d, J = 8.88Hz, 2H, ArH), 7.67 (d, J = 15.54 Hz, 1H, CH), 7.61 (d, J = 15.54 Hz, 1H, CH), 7.29 (dd, J = 3.78, 4.88 Hz, 1H, thiophene-H), 6.84 (d, J = 8.88 Hz, 2H, ArH), 3.83–3.78 (overlapped, 8H, CH_2). ^{13}C NMR (150 MHz, DMSO-d_6) δ: 181.92, 149.30, 146.68, 144.29, 135.15, 133.13, 131.57, 129.29, 123.52, 117.40, 112.47, 52.31, 41.62. HR-MS (ESI) m/z: Calcd for $C_{17}H_{18}Cl_2NOS$ $[M + H]^+$ 354.0486, found 354.0488

3e: Yellow solid, yield 82%. ^{1}H NMR (600 MHz, DMSO-d_6) δ: 8.72 (d, J = 2.22Hz, 1H, thiophene-H), 7.72 (d, J = 8.88Hz, 2H, ArH), 7.76–7.63 (overlapped, 3H, thiophene-H, CH), 7.58 (d, J = 15.38 Hz, 1H, CH), 6.84 (d, J = 8.88 Hz, 2H, ArH), 3.83–3.78 (overlapped, 8H, CH_2). ^{13}C NMR (150 MHz, DMSO-d_6) δ: 183.29, 149.07, 144.05, 143.85, 133.62, 131.37, 137.83, 137.63, 123.59, 118.65, 112.36, 52.24, 41.55. HR-MS (ESI) m/z: Calcd for $C_{17}H_{18}Cl_2NOS$ $[M + H]^+$ 354.0486, found 354.0490

3f: Yellow solid, yield 77%. ^{1}H NMR (600 MHz, DMSO-d_6) δ: 8.05 (d, J = 5.24 Hz, 1H, thiophene-H), 7.70 (d, J = 15.30 Hz, 1H, CH), 7.65 (d, J = 8.88 Hz, 2H, ArH), 7.52 (d, J = 15.30 Hz, 1H, CH), 7.28 (d, J = 5.28 Hz, 1H, thiophene-H), 6.85 (d, J = 8.88 Hz, 2H, ArH), 3.83–3.78 (overlapped, 8H, CH_2). ^{13}C NMR (150 MHz, DMSO-d_6) δ: 181.15, 149.58, 145.49, 137.88, 133.21, 131.51, 131.12, 126.90, 123.12, 118.21, 112.55, 52.23, 41.46. HR-MS (ESI) m/z: Calcd for $C_{17}H_{17}Cl_3NOS$ $[M + H]^+$ 388.0096, found 388.0010

3g: Yellow solid, yield 76%. ^{1}H NMR (600 MHz, DMSO-d_6) δ: 8.30 (d, J = 1.43 Hz, 1H, thiophene-H), 7.98 (d, J = 1.43 Hz, 1H, thiophene-H), 7.71 (d, J = 8.88 Hz, 2H, ArH), 7.65 (d, J = 15.30 Hz, 1H, CH), 7.60 (d, J = 15.30 Hz, 1H, CH), 6.81 (d, J = 8.88 Hz, 2H, ArH), 3.81–3.73 (overlapped, 8H, CH_2). ^{13}C NMR (150 MHz, DMSO-d_6) δ: 181.13, 149.57, 146.69, 145.32, 132.39, 131.86, 129.99, 125.15, 123.44, 116.61, 112.48, 52.29, 41.63. HR-MS (ESI) m/z: Calcd for $C_{17}H_{17}Cl_3NOS$ $[M + H]^+$ 388.0096, found 388.0099

3h: Yellow solid, yield 55%. ^{1}H NMR (600 MHz, DMSO-d_6) δ: 8.18 (d, J = 4.12Hz, 1H, thiophene-H), 7.74 (d, J = 8.88 Hz, 2H, ArH), 7.67 (d, J = 15.30 Hz, 1H, CH), 7.59 (d, J = 15.30 Hz, 1H, CH), 7.35 (d, J = 4.12 Hz, 1H, thiophene-H), 6.84 (d, J = 8.88 Hz, 2H, ArH), 3.85–3.76 (overlapped, 8H, CH_2). ^{13}C NMR (150 MHz, DMSO-d_6) δ: 181.04, 149.42, 145.84, 144.85, 137.49, 133.08, 131.70, 129.45, 123.33, 116.04, 112.39, 52.22, 41.55. HR-MS (ESI) m/z: Calcd for $C_{17}H_{17}Cl_3NOS$ $[M + H]^+$ 388.0096, found 388.0095

3i: Yellow solid, yield 62%. ^{1}H NMR (600 MHz, DMSO-d_6) δ: 7.78 (d, J = 4.96 Hz, 1H, thiophene-H), 7.61 (d, J = 8.88 Hz, 2H, ArH), 7.57 (d, J = 15.25 Hz, 1H, CH), 7.18 (d, J = 15.25 Hz, 1H, CH), 7.08 (d, J = 4.96Hz, 1H, thiophene-H), 6.79 (d, J = 8.88 Hz, 2H, ArH), 7.55–7.52 (overlapped, 2H, thiophene-H, CH), 3.79–3.72 (overlapped, 8H, CH_2), 2.52 (s, 3H, CH_3). ^{13}C NMR (150 MHz, DMSO-d_6) δ: 182.94, 149.26, 144.39, 144.18, 137.43, 133.49, 131.28, 123.33, 119.77, 112.55, 100.00, 52.32, 41.56, 29.51. HR-MS (ESI) m/z: Calcd for $C_{18}H_{20}Cl_2NOS$ $[M + H]^+$ 368.0643, found 368.0648

3j: Yellow solid, yield 66%. ^{1}H NMR (600 MHz, DMSO-d_6) δ: 8.03 (d, J = 1.11Hz, 1H, thiophene-H), 7.68 (d, J = 8.88 Hz, 2H, ArH), 7.60 (d, J = 15.19 Hz, 1H, CH), 7.55–7.52 (overlapped, 2H, thiophene-H, CH), 6.79 (d, J = 8.88 Hz, 2H, ArH), 3.80–3.72 (overlapped, 8H, CH_2), 2.25 (s, 3H, CH_3). ^{13}C NMR (150 MHz, DMSO-d_6) δ: 181.81, 149.25, 146.18, 144.07, 139.31, 135.03, 131.50, 130.62, 123.58, 117.44, 112.46.00, 52.31, 41.62, 15.90. HR-MS (ESI) m/z: Calcd for $C_{18}H_{20}Cl_2NOS$ $[M + H]^+$ 368.0643, found 368.0646

3k: Yellow solid, yield 79%. ^{1}H NMR (600 MHz, DMSO-d_6) δ: 8.06 (d, J = 3.85 Hz, 1H, thiophene-H), 7.71 (d, J = 8.88 Hz, 2H, ArH), 7.62 (d, J = 15.20 Hz, 1H, CH), 7.55 (d, J = 15.20 Hz, 1H, CH), 7.00 (d, J = 3.86Hz, 1H, thiophene-H), 6.83 (d, J = 8.88 Hz, 2H, ArH), 3.82–3.77 (overlapped, 8H, CH_2), 2.53 (s, 3H, CH_3). ^{13}C NMR (150 MHz, DMSO-d_6) δ: 181.38, 149.77, 149.08, 144.50, 143.61, 133.64, 131.39, 127.95, 123.51, 117.17, 112.36, 52.24, 41.55, 16.20. HR-MS (ESI) m/z: Calcd for $C_{18}H_{20}Cl_2NOS$ $[M + H]^+$ 368.0643, found 368.0640

Table S1: The λ_{max}, λ_{em} and stockes shift of the synthetic compounds

Compound	3a	3b	3c	3d	3e	3f	3g	3h	3i	3j	3k
λ_{max}	412	411	392	409	403	410	409	421	421	417	399
λ_{em}	542	524	516	552	546	553	549	566	563	567	529
Stockes shift	130	113	124	143	143	143	140	145	142	150	130

Table S2: Inhibiting concentration 50 (μM) of the synthetic compounds against NCI-H460 and A549 cells

Compound	3a	3b	3c	3d	3e	3f	3g	3h	3i	3j	3k
NCI-H460	25.8±2.4	26.9±1.5	23.1±1.4	28.2±2.1	26.6±3.1	29.8±0.9	26.1±1.3	16.6±0.9	14.2±3.3	15.0±2.2	21.0±1.3
A549	26.3±2.8	27.4±2.6	30.8±2.5	29.7±3.3	28.2±3.4	33.5±2.6	31.8±1.9	13.1±2.7	17.1±4.8	14.6±3.2	25.8±2.4